PERGAMON

Acta mater. Vol. 47, No. 10, pp. 2961–2968, 1999

Printed in Great Britain
PII: S1359-6454(99)00167-6
1359-6454/99 $20.00 + 0.00

SOLIDIFICATION KINETICS AND PHASE FORMATION OF UNDERCOOLED EUTECTIC Ni–Nb MELTS

M. LEONHARDT, W. LÖSER† and H.-G. LINDENKREUZ

Institut für Festkörper- und Werkstofforschung Dresden, Postfach 27 00 16, D-01171 Dresden, Germany

(Received 7 April 1999; accepted 12 May 1999)

Abstract—The non-equilibrium solidification behaviour of undercooled eutectic $Ni_{84}Nb_{16}$ and $Ni_{59.5}Nb_{40.5}$ melts has been analysed by *in situ* observation of recalescence events during electromagnetic levitation of undercooled melts. Levitated drops of controlled undercooling were quenched onto chill substrates and subjected to phase and microstructure analysis. For $Ni_{84}Nb_{16}$ a maximum melt undercooling of 276 K has been achieved. A transition from coupled eutectic to primary supersaturated α-Ni dendrite growth was revealed beyond a critical undercooling of 30 K. Beyond 110 K the primary Ni_3Nb phase occurred for substrate quenching. The undercooling of $Ni_{59.5}Nb_{40.5}$ melt was limited to 135 K. Bulk amorphous samples up to 2 mm thick have been prepared by quenching of undercooled $Ni_{59.5}Nb_{40.5}$ melts. On slow cooling the metastable phases decompose into an anomalous eutectic microstructure. © *1999 Acta Metallurgica Inc. Published by Elsevier Science Ltd. All rights reserved.*

Keywords: Rapid solidification; Nickel alloys; Metallic glasses; Phase transformations

1. INTRODUCTION

Phase selection processes under rapid solidification conditions do not solely depend on alloy composition but on process parameters such as cooling rate, temperature gradient or melt undercooling prior to solidification, too [1, 2]. For various undercooled eutectic alloy systems a gradual transition from lamellar to anomalous eutectic microstructures has been detected beyond a critical melt undercooling $\Delta T_c \approx 200$ K [3–9]. But, no new metastable phase in addition equilibrium phases was detected in the as-solidified bulk undercooled samples, because of the slow post-solidification cooling rate inherent to the common electromagnetic levitation and flux melting techniques applied. Direct evidence for metastable phase formation in Nb–Al [7] and Ni–Si [10] eutectic alloys could be inferred from *in situ* observation of growth kinetics of bulk undercooled melts, which displayed multi-step recalescence processes. The analysis of the metastable phases was accomplished by X-ray diffraction and transmission electron microscopy (TEM) of bulk samples quenched at controlled undercooling levels.

The Ni–Nb phase diagram is distinguished by two different eutectic compositions $Ni_{84}Nb_{16}$ and $Ni_{59.5}Nb_{40.5}$, respectively [11]. It is presented in Fig. 1 along with metastable extensions of liquidus, solidus and T_0-lines relevant for non-equilibrium solidification processes [12]. The two eutectic compositions differ in the character of the terminal equilibrium phases, the f.c.c. α-Ni solid solution and the ordered orthorhombic Ni_3Nb phase on the one hand ($Ni_{84}Nb_{16}$), and the ordered orthorhombic Ni_3Nb and rhombohedral Ni_6Nb_7 phases, on the other hand ($Ni_{59.5}Nb_{40.5}$). Therefore, we may anticipate a quite different non-equilibrium solidification behaviour of the two eutectic Ni–Nb alloy compositions. Previous drop tube solidification experiments of eutectic $Ni_{60}Nb_{40}$ alloys have yielded an amorphous phase fraction, which predominates for small particle sizes of 20–30 μm [13]. An undercooling level of 500 K was presumed to be necessary for glass formation in gas atomized $Ni_{60}Nb_{40}$ particles.

In this paper, undercooled eutectic Nb–Ni melts are studied by an electromagnetic levitation technique allowing for *in situ* observation of the solidification process along with quenching of undercooled samples on chill substrates. In that way the primary solidification mode and microstructure formation mechanisms are elucidated. Results are compared with predictions of solidification models.

2. EXPERIMENTAL METHODS

Master alloys of eutectic Ni–Nb compositions were prepared from 99.99% pure Ni and Nb in an arc melting furnace on a water cooled copper crucible under Ar atmosphere. Samples of about 1.0 g mass, corresponding to spheres of 6 mm diameter, were investigated by means of electromagnetic levitation experiments. A comprehensive description of the type of levitation facility used is given

†To whom all correspondence should be addressed.

elsewhere [7, 14]. The vacuum chamber was evacuated to 10^{-8} mbar and refilled with purified 6 N He/H_2 gas. The samples were repeatedly molten in that atmosphere and cooled by a gas stream enabling cooling velocities up to ~50 K/s. The temperature of the sample was monitored by a two-colour pyrometer at a sampling rate of 50 Hz with an accuracy of < 3 K. The solidification of the melt is initiated by triggering with a ceramic substrate at a controlled undercooling. In order to resolve details of the temperature–time characteristics during the fast recalescence period the temperature of a $1.0 \times 1.0\ mm^2$ large section of the drop surface was projected onto a fast responding silicon photodiode. The equipment permits recording with sampling rates of 1.5 MHz. The dendrite growth velocities were determined by measuring the time needed for the solidification front to sweep across the sample surface.

Melt drops of well-defined undercooling level were quenched onto a copper substrate or, alternatively, onto a copper substrate coated with tin solder in order to enhance the interfacial heat transfer. Immediately after nucleation the drops solidify with a preferred heat flow into the undercooled melt but a subsequent heat transfer into the substrate. This permits high cooling rates of up to ~10^5 K/s at least in a layer adjacent to the chill substrate.

The phase content of as-solidified specimens was analysed by X-ray diffraction utilizing the Cu-K_α line. The microstructure of as-solidified samples was revealed by optical microscopy and scanning electron microscopy (SEM). Electron probe microanalysis (EPMA) point scans of Ni were performed in the energy-dispersive mode (EDX) and wavelength-dispersive mode (WDX) in order to identify the local compositions of selected microstructure elements. Special care was devoted to the question of sample pollution, which could arise from the melting substrate interface layer. No concentration of Sn exceeding 0.1 at.% was detected in quenched samples near the substrate either by EDX or by secondary ion mass spectrometry. In addition, some sample sections were subjected to ion beam thinning and investigated by TEM. Differential scanning calorimetry (DSC) runs were conducted in order to reveal the transformation temperatures of the metastable phases.

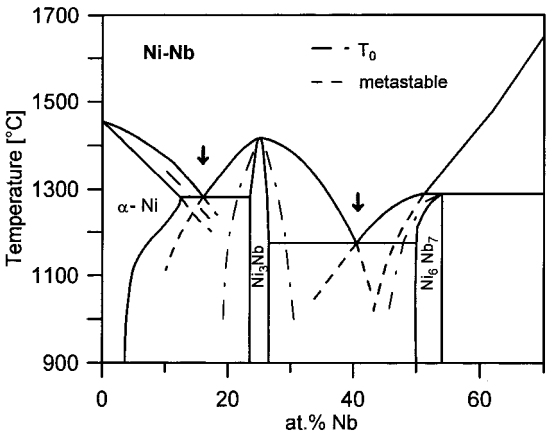

Fig. 1. Ni–Nb phase diagram according to Ref. [11]. Dashed lines: metastable extensions of liquidus and solidus lines. Dash-dotted lines: estimated T_0-lines. Arrows denote the two alloy compositions investigated.

3. EXPERIMENTAL RESULTS

3.1. Time–temperature characteristics of the solidification process

The maximum undercooling of levitated $Ni_{84}Nb_{16}$ melt drops achieved in the He/H_2 gas flow was 286 K. The recalescence process proceeds within a time interval of the order of 1 ms and can be considered as adiabatic. As shown in Fig. 2 beyond a critical undercooling of $\Delta T_c \geq 30$ K there was transition to a characteristic two-step recalescence behaviour of $Ni_{84}Nb_{16}$ undercooled samples with an arrest time near $\Delta T \approx 15$ K undercooling. The solidification velocity vs undercooling relationship derived from the primary recalescence step of $Ni_{84}Nb_{16}$ melts is shown in Fig. 3. All data points are traced from trigger experiments which allow for a definite geometry and exhibit much less scatter in experimental data than spontaneous recalescence events. There is a monotonous rise of the velocity with undercooling from $v = 0.06$ m/s for $\Delta T = 30$ K up to 4.7 m/s for $\Delta T = 275$ K. The magnitude of the velocity exceeds that predicted for coupled eutectic growth but is rather typical for dendrite growth. The experimental results are compared with calculated dendrite tip velocity vs ΔT curves of the α-Ni phase according to the Lipton–Kurz–Trivedi

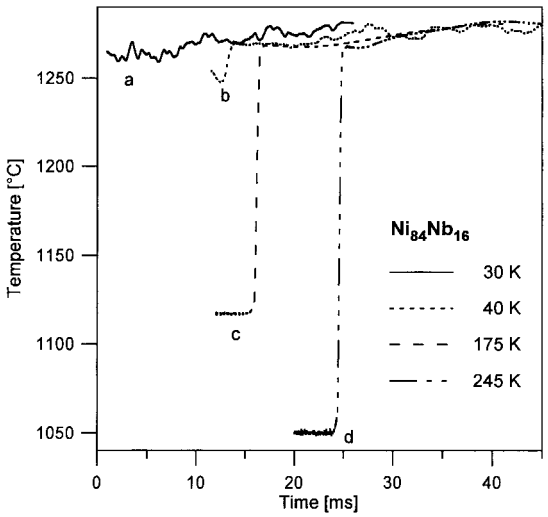

Fig. 2. Temperature–time characteristics of recalescence events of eutectic $Ni_{84}Nb_{16}$ melt samples with various undercooling: (a) $\Delta T = 30$ K; (b) $\Delta T = 40$ K; (c) $\Delta T = 175$ K; (d) $\Delta T = 245$ K.

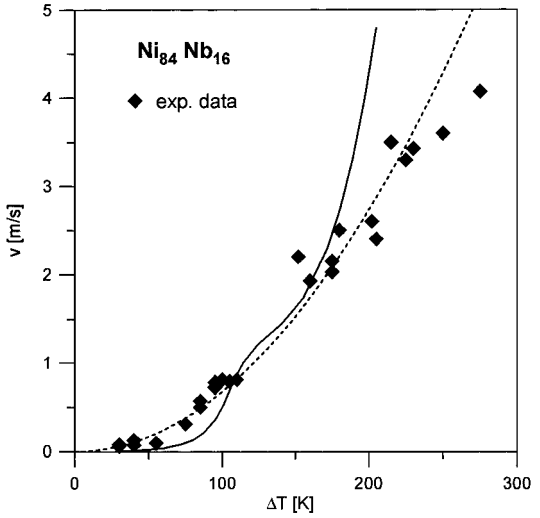

Fig. 3. Experimentally determined dendrite growth velocity vs melt undercooling of levitated $Ni_{84}Nb_{16}$ drops (◆, dashed line) and dendrite growth velocities calculated from the LKT model with parameters given in Table 1 (solid line).

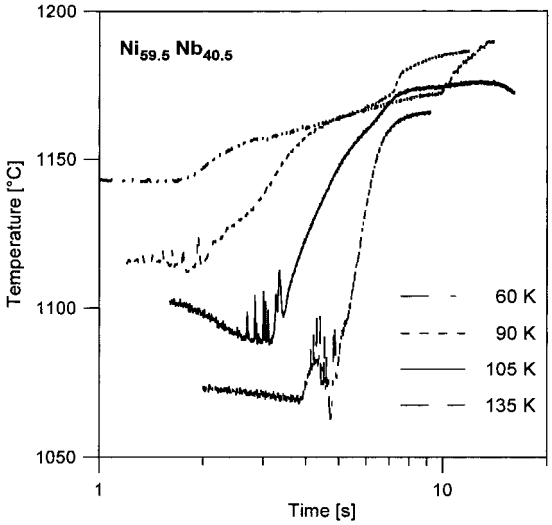

Fig. 4. Temperature–time characteristics of recalescence events of undercooled eutectic $Ni_{59.5}Nb_{40.5}$ melts: (a) $\Delta T = 60$ K; (b) $\Delta T = 90$ K; (c) $\Delta T = 105$ K; (d) $\Delta T = 135$ K.

(LKT) theory of dendrite growth in bulk undercooled melts [15]. The model calculation involves a velocity dependence of partition coefficient and liquidus slope, respectively. The parameters utilized in the calculation are given in Table 1. We refer to textbooks for the basic equations [16]. The course and the magnitude of the experimentally observed v vs ΔT behaviour are consistent with the supposed dendrite growth of α-Ni solid solution. The steep rise in the calculated velocity near $\Delta T \approx 100$ K is ascribed to the transition from diffusion to thermally controlled dendrite growth due to solute trapping.

For $Ni_{59.5}Nb_{40.5}$ samples there was a relatively smooth increase of the temperature–time plots Fig. 4. There is a sluggish recalescence process. The recalescence times of the undercooled $Ni_{59.5}Nb_{40.5}$ melts are of the order of seconds, i.e. they exceed those of the $Ni_{84}Nb_{16}$ alloy discussed above by three orders of magnitude. Moreover, from the video images there was no apparent single solidification front passing the sample. Therefore, we were not able to derive a distinct solidification velocity like in the former case. For melt undercooling between $\Delta T = 50$ and 105 K recalescence events exhibited different steps with duration of several seconds. Because of the long duration of the recalescence process there was an indication for non-adiabatic behaviour.

Table 1. Parameters used for calculations of the dendrite tip velocity of $Ni_{84}Nb_{16}$

Quantity	Value
Specific heat of the melt	600 J/kg K
Latent heat of fusion	2.9×10^5 J/kg
Interdiffusion coefficient of the melt	6×10^{-9} m^2/s
Initial melt composition	16 at.%
Melting temperature	1555 K
Thermal diffusivity of the melt	2×10^{-6} m^2/s
Gibbs–Thompson parameter	3.1×10^{-7} m K
Liquidus slope of α-Ni	−16 K/at.%
Equilibrium partition coefficient	0.78
Length unit for solute trapping	5×10^{-9} m
Velocity of sound	3000 m/s

3.2. Microstructure and phase analysis of $Ni_{84}Nb_{16}$ samples

Microstructure, composition and structure of the phases have been determined in the as-solidified samples, which were quenched from controlled undercooling levels. From the equilibrium phase diagram [11] we expect a co-operative growth of the eutectic α-Ni + Ni_3Nb two-phase microstructure

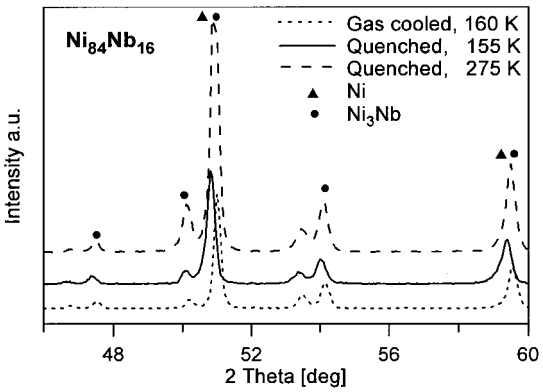

Fig. 5. X-ray diffraction diagrams of as-solidified $Ni_{84}Nb_{16}$ samples of different undercooling levels prior to solidification and post-solidification cooling, respectively: (a) $\Delta T = 160$ K, gas cooled; (b) $\Delta T = 155$ K, quenched on Sn-coated substrate; (c) $\Delta T = 275$ K, quenched on Sn-coated substrate. Reflections of α-Ni (▲) and Ni_3Nb (●) are indicated.

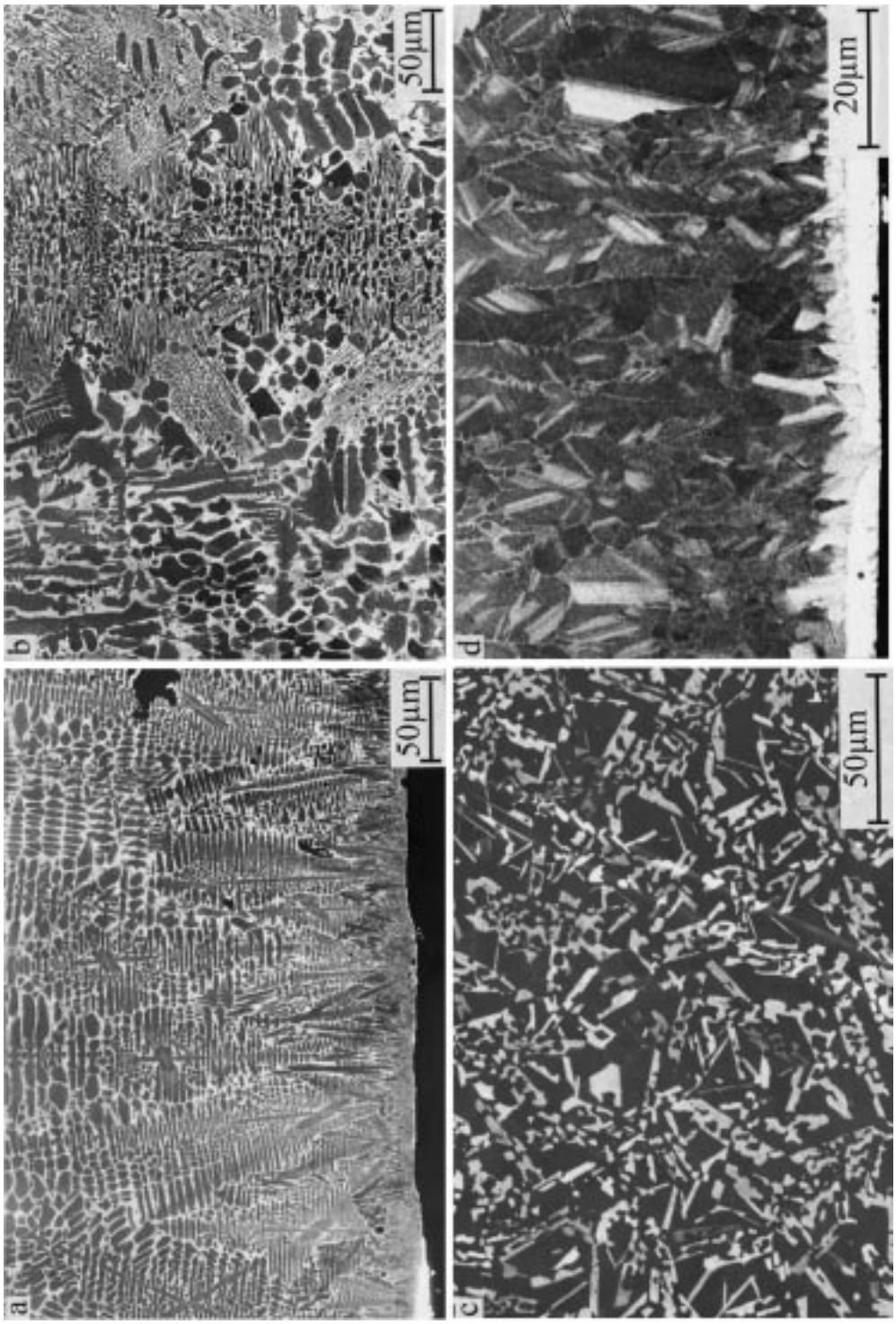

Fig. 6. Cross-sectional SEM micrograph of as-solidified $Ni_{84}Nb_{16}$ samples for different undercooling levels prior to solidification and post-solidification cooling, respectively: (a) $\Delta T = 70$ K, quenched on a Cu substrate (bottom): metastable α-Ni dendrites (dark); (b) $\Delta T = 70$ K, central part of the sample quenched on a Cu substrate: dendritic microstructure along with lamellar eutectic [α-Ni (dark) + Ni_3Nb (bright)] cells in interdendritic regions; (c) $\Delta T = 160$ K, gas cooled: anomalous eutectic α-Ni + Ni_3Nb microstructure; (d) $\Delta T = 240$ K, quenched on a Sn-coated substrate: Ni_3Nb phase layer (bright) near the chill substrate interface (bottom) succeeded by a weakly segregated twinned α-Ni microstructure (greyish).

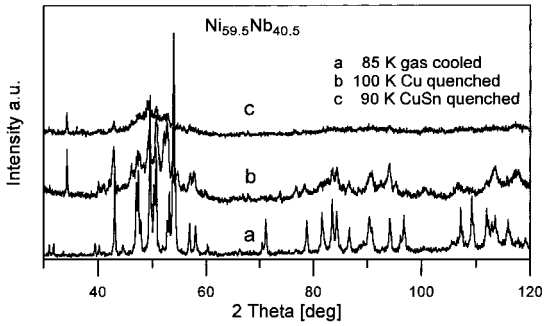

Fig. 7. X-ray diffraction diagrams of as-solidified undercooled $Ni_{59.5}Nb_{40.5}$ samples subjected to different post-solidification cooling methods: (a) $\Delta T = 85$ K, slow gas cooling (10 K/s); (b) $\Delta T = 100$ K, quenching on Cu substrate; (c) $\Delta T = 90$ K, quenching on Sn-coated Cu substrate.

for the $Ni_{84}Nb_{16}$ alloy. Indeed, the X-ray diffraction patterns of both the directionally solidified ingots and levitated samples display no trace of any metastable phase in addition to the f.c.c. α-Ni and the orthorhombic Ni_3Nb phase reflections (Fig. 5). There is some shift of the α-Ni peaks corresponding to a change of the f.c.c. lattice parameters from $a = 0.352$ nm for as-cast samples toward $a = 0.361$ nm after quenching. This is due to the enhanced Nb supersaturation and may be compared with results of ordinary melt quenching experiments [17].

As demonstrated by the SEM micrographs the lamellar microstructure of the master alloy, which is also apparent in gas-cooled samples with small undercooling prior to solidification, is replaced by a dendritic microstructure [Fig. 6(a)] in quenched samples beyond a relatively moderate undercooling of 30 K prior to solidification. The dendritic α-Ni supersaturated solid solution phase occurred upon quenching onto a Cu substrate for undercooling levels of $30\,\text{K} < \Delta T < 105\,\text{K}$. It was revealed by EPMA that the dendrite composition adjacent to the substrate interface was near to the eutectic melt composition. Neither for the segregated dendritic structure above this layer nor for the anomalous eutectic in the remaining sections did the constituent phases achieve their equilibrium composition. More distant from the substrate lamellar eutectic cells were detected in interdendritic regions which result from the residual solidification [Fig. 6(b)]. Gas cooled samples with moderate and high undercooling levels prior to solidification exhibited the anomalous eutectic α-Ni + Ni_3Nb microstructure [Fig. 6(c)]. For samples quenched from undercooling levels exceeding 110 K onto a Sn-coated Cu substrate, however, we observed another change in the solidification mode. The orthorhombic Ni_3Nb phase was detected as a uniform layer of 10 μm thickness [for samples with $\Delta T = 275$ K, see Fig. 6(d)] adjacent to the chill substrate. The orthorhombic crystal structure of that phase has been identified by TEM nanodiffraction patterns. Its composition was about 17 at.% Nb, slightly beyond the eutectic melt composition as inferred from EPMA but strongly deviates from the Ni_3Nb stoichiometry. Above that layer a weakly segregated dendritic microstructure primarily consisting of the α-Ni phase had developed succeeded by anomalous and lamellar eutectic regions more distant from the chill substrate.

3.3. X-ray analysis, microstructure, and transformation behaviour of $Ni_{59.5}Nb_{40.5}$ samples

The solidification behaviour and microstructure of undercooled $Ni_{59.5}Nb_{40.5}$ samples is completely distinct from the $Ni_{84}Nb_{16}$ alloy and, moreover, there is an apparent change in microstructure of samples subjected to different cooling conditions. As demonstrated by the X-ray diffraction patterns in Fig. 7 the phase content of samples solidified from 85 to 100 K undercooling is changed from the equilibrium Ni_3Nb + Ni_6Nb_7 phases for slowly gas-cooled samples to a partial amorphous structure for the substrate-quenched specimen. The amorphous fraction severely depends upon the kind of chill substrate. Bulk amorphous Ni–Nb samples of nearly 2 mm thickness have been achieved by quenching undercooled droplets onto a tin-coated Cu substrate. Even samples with medium cooling rates (achieved by vigorous gas convection) displayed small fractions of an amorphous phase. Characteristic microstructures of samples from SEM investigations are illustrated in Fig. 8. A two-phase (Ni_3Nb + Ni_6Nb_7) microstructure [Fig. 8(a)] of the gas-cooled sample was revealed consisting of lamellar and anomalous eutectic regions, respectively. In samples quenched onto copper chill substrates a featureless amorphous layer was formed adjacent to the substrate. Its thickness increased with the undercooling level. Niobium-enriched spheroids were detected near the boundary between the amorphous layer adjacent to the chill substrate and the remaining part, which consists of weakly segregated dendrites for specimens quenched from $\Delta T \approx 40$ to 115 K [Fig. 8(b)]. Undercooled droplets quenched onto tin-coated chill substrates with improved interfacial heat transfer exhibit the predominant amorphous structure with a featureless appearance for a thickness up to 2 mm [Fig. 8(c)]. Small precipitates of a phase with 60–66 at.% Nb were detected, which formed isolated randomly oriented dendrites within the glassy matrix or sharply edged small inclusions near regions with poor substrate contact [Fig. 8(c)] and at the air side of quenched amorphous samples [Fig. 8(d)], respectively. The structure of that minority phase fraction could not be identified by X-ray diffraction. A segregated microstructure was revealed in the sample if some critical distance from the chill substrate is exceeded [Fig. 8(d)].

As-quenched amorphous samples were subjected to isochronal annealing with a heating rate of 10 K/

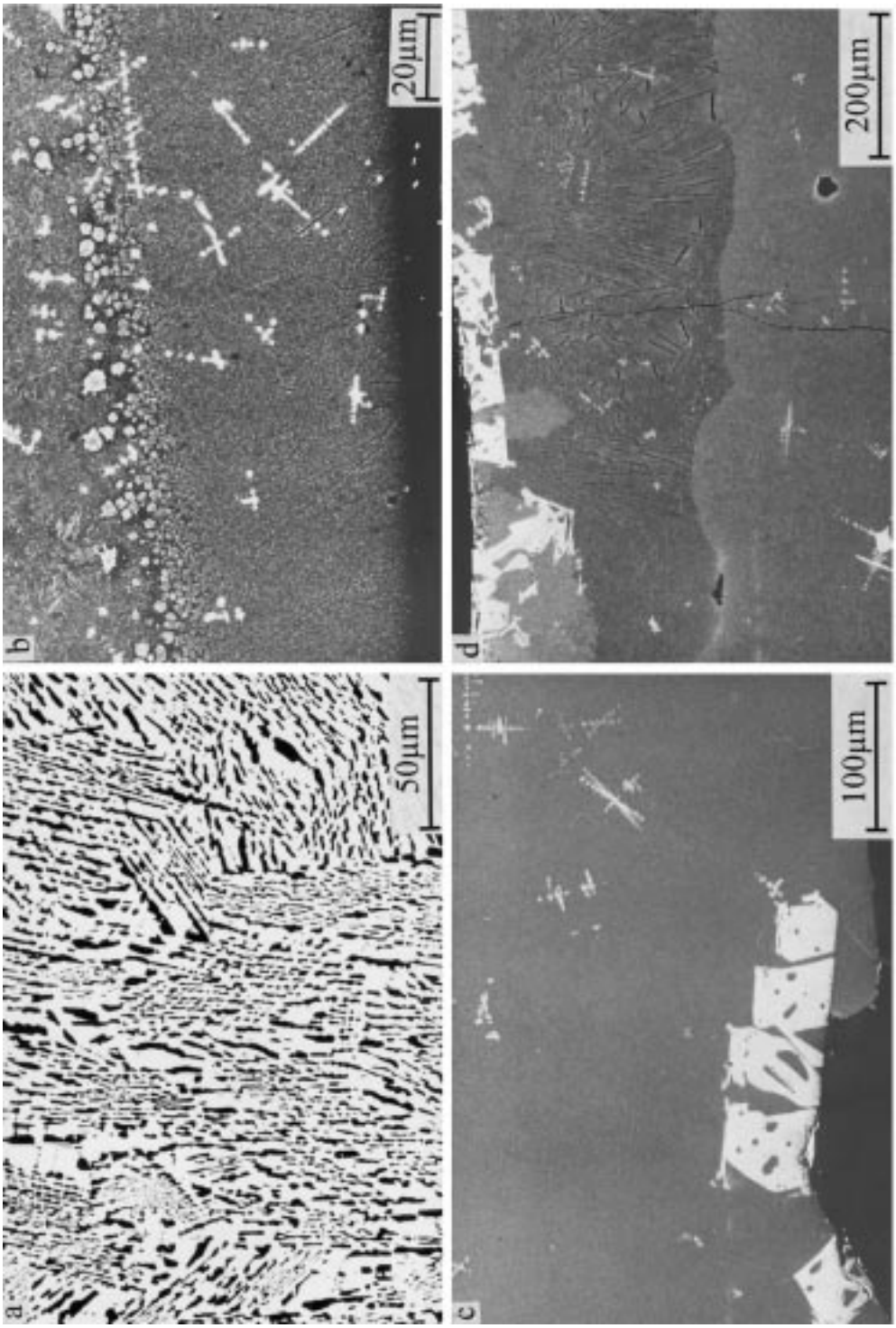

Fig. 8. Cross-sectional SEM micrograph of as-solidified undercooled $Ni_{59.5}Nb_{40.5}$ samples subjected to different post-solidification cooling methods: (a) $\Delta T = 85$ K, slow gas cooling: Ni_3Nb (dark) + Ni_6Nb_7; (b) $\Delta T = 70$ K, quenching on Cu substrate: transition from amorphous layer (bottom) to crystalline microstructure (bright: precipitation of a Nb-rich phase); (c) $\Delta T = 90$ K, quenching on Sn-coated Cu substrate (bottom): featureless amorphous structure with Nb-rich phase inclusions in regions with poor substrate contact; (d) $\Delta T = 90$ K, quenching on Sn-coated Cu substrate: transition from featureless amorphous structure to a segregated microstructure and precipitation of a Nb-rich phase near the air-side (top).

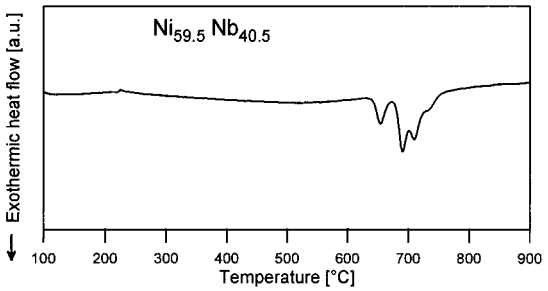

Fig. 9. DSC plots for isochronal heating with 5 K/s of bulk amorphous $Ni_{59.5}Nb_{40.5}$ samples ($\Delta T = 90$ K, quenched on Sn-coated Cu substrate). Exothermal crystallization beyond 630°C.

min. Three exothermic crystallization peaks with onset temperatures between 642 and 680°C were detected (Fig. 9). They correspond to the decay of the amorphous matrix. A lamellar Ni_3Nb + Ni_6Nb_7 microstructure of resolidified DSC samples was achieved.

4. DISCUSSION AND CONCLUSIONS

The results of growth kinetics along with microstructure investigations of samples quenched at controlled undercooling levels, offered the unique possibility to track the solidification pathway of undercooled eutectic Ni–Nb melts. One interesting result was the striking difference between the two eutectic alloy compositions within the Ni–Nb system, which is seemingly due to the character of the terminal equilibrium phases.

The transition from eutectic to primary dendrite solidification was found for $Ni_{84}Nb_{16}$ beyond a relatively small critical undercooling of $\Delta T_c \approx 30$ K which is consistent with the T_0-temperature of the α-Ni phase extrapolated to the eutectic composition. Accordingly, the metastable supersaturated α-Ni dendrites have been identified in quenched samples. The second temperature rise after the primary solidification is ascribed to the residual eutectic solidification. For undercooled samples exposed to slow gas cooling the dendritic microstructure is apparently transformed into the anomalous eutectic structure, which covers the whole sample cross section for large undercooling. A primary Ni_3Nb phase solidification in samples substrate-quenched from undercooling levels >110 K could arise. The concentration of that metastable phase 17 at.% Ni matches with the maximum composition inferred from the calculated T_0-line of the Ni_3Nb phase [12]. Generally, for the solidification of a metastable ordered Ni_3Nb phase one would expect an additional thermal arrest in the recalescence characteristic and possibly a sudden drop in the solidification velocity near the critical undercooling [18]. However, there was no apparent change in the recalescence behaviour of the levitated sample. Therefore, we must suppose that the observed change in solidification mode is initiated by heterogeneous nucleation of the substrate. Substantial differences in phase selection between spontaneous nucleation and triggered solidification of undercooled melts has already been reported in various other alloy systems such as Fe–Ni [19], Fe–Cr–Ni [20, 21] and Nd–Fe–B [22].

In $Ni_{59.5}Nb_{40.5}$ melts a relatively low maximum undercooling of 135 K has been achieved. The undercooled eutectic $Ni_{59.5}Nb_{40.5}$ melt differs from many other alloys investigated by its peculiar recalescence behaviour and the glass formation tendency. The alloy is known to form a stable amorphous structure with one of the highest crystallization temperatures (637°C) among the metallic glasses [23]. However, it seems to be the first time that bulk amorphous samples exceeding 1 mm thickness have been prepared from a binary alloy. This has been accomplished by undercooling the melt prior to quenching onto a chill substrate. Eutectic alloys with plunging T_0-curves of the constituent phases are good candidates for easy metallic glass formation [24] since no crystalline phase can compete in the undercooled melt. The Ni–Nb phase diagram features near the eutectic $Ni_{59.5}Nb_{40.5}$ composition suggests this behaviour [11, 12]. The experimentally determined melt undercooling of the order of 100 K necessary for glass formation of $Ni_{59.5}Nb_{40.5}$ is surprisingly low compared with the estimated 500 K undercooling for glass formation of fine particles in drop tube experiments [13]. However, effective post-solidification cooling of samples is mandatory since otherwise crystalline or partially amorphous microstructures may result. Within the amorphous matrix some Nb-rich phase precipitates occurred. The formation of Nb-rich metastable phases on the primary crystallization step of amorphous Ni–Nb alloys has been reported by Busch [12]. Knowing the glassy structure of as-quenched $Ni_{59.5}Nb_{40.5}$ samples one can interpret the recalescence events of undercooled samples subjected to slow gas cooling during the levitation process. In that case the slow post-solidification cooling rate of the order of 10 K/s (near 1000°C) is not sufficient to retain the glassy state. The heat release during the crystallization process of the metallic glass will cause the relatively slow recalescence of the levitated $Ni_{59.5}Nb_{40.5}$ samples. Whereas a succeeding eutectic solidification of the residual melt may give rise to double-recalescence events. This is in accordance with the observed microstructure of the slowly cooled samples, which consist of the equilibrium phases and exhibit a mixture of anomalous and lamellar eutectic morphology. The current investigation has stressed both the effect of constitution and process parameters on the metastable phase formation and microstructure of rapidly solidified Ni–Nb eutectic alloys.

Acknowledgements—We would like to D. M. Herlach, J. Eckert and R. Busch for valuable discussions and I. Stange, B. Arnold and H. Schulze for experimental assistance. The authors express their gratitude for financial support from Deutsche Forschungsgemeinschaft Contract-No. Lo 548/2-2.

REFERENCES

1. Herlach, D.M., *Mater. Sci. Engng*, 1994, **R12**, 177.
2. Kurz, W. and Trivedi, R., *Mater. Sci. Engng*, 1994, **A179/A180**, 46.
3. Wei, B. and Herlach, D. M., *Adv. Mater.*, Vol. I. Elsevier Science, Amsterdam, 1993, p. 639.
4. Kattamis, T.Z. and Flemings, M.C., *Metall. Trans.*, 1970, **1**, 449.
5. Wei, B., Herlach, D.M., Feuerbacher, B. and Sommer, F., *Acta metall. mater.*, 1993, **41**, 1801.
6. Wei, B., Herlach, D.M. and Sommer, F., *J. Mater. Sci. Lett.*, 1993, **12**, 1774.
7. Löser, W., Hermann, R., Leonhardt, M., Stephan, D. and Bormann, R., *Mater. Sci. Engng*, 1997, **A224**, 53.
8. Abbaschian, R. and Lipschutz, M.D., *Mater. Sci. Engng*, 1997, **A226-228**, 13.
9. Goetzinger, R., Ph.D. thesis, Ruhruniversität Bochum, 1998.
10. Leonhardt, M., Löser, W. and Lindenkreuz, H.-G., *Mater. Sci. Engng A*, 1999, in press.
11. Kattner, U. R., in *Binary Alloy Phase Diagrams*, ed. T. B. Massalski. American Society for Metals, Metals Park, OH, 1986, p. 180.
12. Busch, R., Diploma thesis, Universität Göttingen, 1988.
13. Shong, D. S., Graves, J. A., Ujiie, Y. and Perepezko, J. H., *Mater. Res. Symp. Proc.*, Vol. 87. Materials Research Society, Pittsburgh, PA, 1987, p. 17.
14. Löser, W., Genest, H. and Lindenkreuz, H.-G., Ann. Report, Institut für Festkörper- und Werkstofforschung Dresden, 1994, p. 27.
15. Lipton, J., Kurz, W. and Trivedi, R., *Acta metall.*, 1987, **35**, 957.
16. Kurz, W. and Fisher, D. J., *Fundamentals of Solidification*. Trans Tech Publications, Aedermannsdorf, 1992, p. 133ff.
17. Ruhl, R.C., Giessen, B.C., Cohen, M. and Grant, N.J., *J. less-common Metals*, 1967, **13**, 611.
18. Löser, W., Garcia-Escorial, A. and Vinet, B., *Int. J. Non-Equilibrium Processing*, 1998, **11**, 89.
19. Schleip, E., Herlach, D.M. and Feuerbacher, B., *Europhys. Lett.*, 1990, **11**, 751.
20. Löser, W., Volkmann, Th. and Genest, H., *Proc. 4th European Conf. Adv. Mater. and Processes (EUROMAT 95)*, Padua/Venice, 25–28 September 1995, Symposium F—Materials and Processing Control. Assozione Italiana di Metallurgia, Milano, 1995, p. 147.
21. Koseki, T. and Flemings, M.C., *Metall. Mater. Trans.*, 1998, **28A**, 2385.
22. Hermann, R. and Löser, W., *J. appl. Phys.*, 1998, **83**, 6399.
23. Chen, H. S. and Jackson, K. A., *Metallic Glasses*. American Society for Metals, Metals Parks, OH, 1976, p. 74.
24. Perepetzko, J. H. and Boettinger, W. J., *Mater. Res. Soc. Symp. Proc.*, Vol. 19. Materials Research Society, Pittsburg, PA, 1983, p. 223.